Biosensors and Bioelectronics 53 (2014) 377–383

Contents lists available at ScienceDirect

Biosensors and Bioelectronics

journal homepage: www.elsevier.com/locate/bios

Label-free and ultrasensitive microRNA detection based on novel molecular beacon binding readout and target recycling amplification

Haifeng Dong [a], Kaihong Hao [a], Yaping Tian [b], Shi Jin [a], Huiting Lu [a], Shu-Feng Zhou [c], Xueji Zhang [a,*]

[a] Research Center for Bioengineering and Sensing Technology, University of Science & Technology Beijing, Beijing 100083, PR China
[b] Department of Clinical Biochemistry, Chinese PLA General Hospital, 28 Fuxing Road, Beijing 100853, PR China
[c] Department of Pharmaceutical Sciences, College of Pharmacy, University of South Florida, Tampa, FL 33612, USA

ARTICLE INFO

Article history:
Received 8 July 2013
Received in revised form
10 September 2013
Accepted 20 September 2013
Available online 8 October 2013

Keywords:
MicroRNA detection
Oligonucleotide-stabilized Ag nanoclusters
Target recycling
Molecular beacon

ABSTRACT

A label-free and high-sensitive microRNA (miRNA) detection approach by coupling a metal ion-meditated conformational molecular beacon (MB), using novel fluorescent Ag nanocluster (AgNCs) as fluorophore, with endonuclease-assisted target recycling amplification was developed. The assay comprised an Hg^{2+} ion-meditated conformational MB probe and an assistant probe that do not hybridize with each other at a specific temperature and can be annealed to each other in the presence of the target to form a Y-shape junction structure and released Hg^{2+}. The target-MB hybridization event with the help of assistant probe can readily be read out based on the efficient fluorescence quenching of AgNCs by released Hg^{2+}, while the Y-shape junction structure consisting of the probe MB, assistant probe and target miRNA could be recognized by the endonuclease Nt.BbvCI. The MB probe was then effectively cleaved by the endonuclease, and the regenerated assistant probe and the target further attended another cleavage cycle to implement the signal amplification. The competition displacing interaction between the target and the Hg^{2+} endows the biosensor with high sequence discrimination capability, while the high signal-to-noise ratio and target recycling amplification allows the biosensor to detect the target with high sensitivity. Under the optimal conditions, the concentration of target miRNA could be conveniently read out with a linear range from 10 pM to 1 fM. The proposed approach, avoiding any laborious label, possessing high sensitivity and selectivity, provided significant potential applications in future clinical analysis.

1. Introduction

MicroRNAs (miRNAs) comprise a class of noncoding 18–25 nucleotide RNAs in the genomes of different species (Mallory and Vaucheret, 2006; He and Hannon, 2004; Cissell et al., 2007). Researchers have discovered that miRNAs regulated a wide range of biological processes (Pasquinelli et al., 2005; Lewis et al., 2005; Plasterk, 2006), including cell differentiation, proliferation, and apoptosis at the post-transcriptional levels through mediating mRNA cleavage or preventing protein synthesis (Bartel, 2004; Ambros, 2004). Specifically, it is widely believed that aberrant miRNA levels are associated with various cancers (Calin and Croce, 2006; Jeffrey, 2008; Lu et al., 2006). Therefore, miRNA is emerging as a group of clinically significant diagnostic and prognostic markers as well as useful candidates or targets in therapeutic intervention and basic biomedical research (Jay et al., 2007; Kumar et al., 2007; Tricoli and Jacobson, 2007). However, profiling miRNA expression is technically challenging due to their intrinsic characteristics such as the short sequence lengths, low abundance, and high sequence similarity of miRNAs (Wark et al., 2008; Dong et al., 2012a). Numerous complicated technical variants are needed for conventional RNA analysis including Northern blotting, reverse transcriptase polymerase chain reaction, and microarrays to adapt the specific challenges of miRNA analysis (Pall et al., 2007; Nelson et al., 2004). Various reliable and cost effective miRNA detection methods become attractive and paramount for miRNA expression analysis (Dong et al., 2012b), for example, a simple and cost-effective miRNA detection strategy was designed by combing target assisted isothermal exponential amplification with fluorescent DNA-scaffolded Ag nanocluster (AgNCs) (Liu et al., 2009, 2012).

Molecular beacon (MB) is a single-stranded oligonucleotide hybridization probe with a fluorophore-quencher pair covalently linked to its 5′- and 3′- termini. Upon hybridization with the target, the MB undergoes a spontaneous conformational reorganization, which forces the stem apart and causes the fluorophore and the quencher to separate from each other, leading to the

* Corresponding author. Tel./fax: +86 10 82375840.
E-mail address: zhangxueji@ustb.edu.cn (X. Zhang).

0956-5663/$ - see front matter © 2013 Elsevier B.V. All rights reserved.
http://dx.doi.org/10.1016/j.bios.2013.09.061

restoration of fluorescence for detection (Tyaji and Kramer, 1996; Marras, 2006). As a typical solution-based hybridization assay for nucleic acid detection, it has attracted great attention due to unique thermodynamics, high selectivity, and rapid hybridization kinetics (Sokol et al., 1998; Li et al., 2000; Tang et al., 2005). However, MB also suffers from some inherent deficiencies. Firstly, simplifying the complicate and laborious probe design, synthesis and double-labeling is a still great challenge. Efficient signal-transduction strategies are urgently needed to improve the performance of the MB. For example, Wang et al. proposed metal ions-mediated conformational switch and label-free MB-based strategy using competitive displacement interaction (Wang et al., 2009; Wang et al., 2010). Pumera et al. designed a sensitive impedimetric genosensing platform by combing the graphene with hairpin-DNA structure, which showed high capability of discriminating sequence mismatch (Bonanni and Pumera, 2011). Secondly, the ineffective quenching efficiency will produce a false-positive signal and limit the sensitivity; the limit of the detection based on MB-based methods in molecular is always nanomolar level, which limits its wide application (Tyaji and Kramer, 1996; Marras, 2006). The choices of fluorophores and quenchers are imperative (Dyadyusha et al., 2005). For example, quantum dots and gold nanostructures have been used as the fluorophores and quenchers of MB for sequence-specific DNA detection (Oh et al., 2005; Wang et al., 2009). A novel MB-based molecular detection platform has been developed using graphene oxide as the quencher of quantum dot fluorophore (Dong et al., 2010). Recently, noble metal nanoclusters comprising a few to tens of atoms are emerging as a class of promising fluorophores (Zheng et al., 2007; Duan and Nie, 2007; Rao and Pradeep, 2010), and attracting special attention in the production of an optical biosensor (Petty et al., 2011; Petty et al., 2012). It was demonstrated that the Hg^{2+} ion could efficiently quench the fluorescence of silver nanoclusters (AgNCs) (Guo et al., 2009), which would interest us to explore the AgNCs and Hg^{2+} as novel fluorophores and quenchers of MB. Finally, detection of biomolecules with high sensitivity remains a great encumbrance, which limits the broad application of the MB-based methods in miRNA analysis. The low abundance of miRNA requires efficient signal amplification strategy to be introduced in the MB-based detection.

Here, a convenient miRNA and high sensitive miRNA detection platform was developed by integrating label-free mercury ion-meditated conformational MB using novel fluorescent AgNCs as fluorophore with endonuclease assisted target recycling for signal amplification. As shown in Fig. 1A, the Y-shape junction structure has three complementary oligonucleotide branches and contains a duplex structure recognized by the endonuclease Nt.BbvCI. Hg^{2+} meditated conformational MB probe does not hybridize with the target at a specific temperature (Fig. 1B). In the presence of assistant probe, the target and MB can be annealed to each other to form a Y-shape junction structure and released Hg^{2+}(Fig. 1C). The binding event of label-free MB with its miRNA target with the help of assistant probe can then be read out through the efficient fluorescence quenching of AgNCs by released Hg^{2+}. Meanwhile, the formation of Y-structure can be recognized by the endonuclease Nt.BbvCI, which then efficiently cleaves the MB probe and regenerates the target and assistant probe. These regenerated agents further attend another cleavage cycle to realize the signal amplification. It is worthy to mention that, in the proposal system, the use of the assistant probe could circumvent the sequence limitation coming from the target sequence of Nt.BbvCI, and makes it possible to be widely used in nucleic acid analysis. The competition displacing interaction between the target and the Hg^{2+} endows the biosensor high sequence discrimination capability, while the high signal-to-noise ratio and the target recycling signal amplification leads to a notable sensitivity improvement by more than 10^6 times compared to the traditional MB-based methods in molecular detection with a limit of 25 nM. The proposed method was simple-designed and cost-effective while avoiding complicated temperature control (Liu et al., 2012) and any laborious labeling, and which provided significant potential applications in clinical analysis.

2. Experimental section

2.1. Materials and reagents

Sodium borohydride ($NaBH_4$), silver nitrate ($AgNO_3$), and citric acid were purchased from Sinopharm Chemical Reagent Co. Ltd (China). Nicking endonuclease (NE) Nt.BbvCI (10,000 units/mL) and NE buffer (50 mM potassium acetate, 20 mM Tris-acetate, 10 mM magnesium acetate 100 μg/mL BSA) were purchased from New England Biolab®. Ultrapure water obtained from a Millipore water purification system (≥ 18 MΩ, Milli-Q, Millipore, Billerica, MA) was used in all runs. All other reagents were of analytical grade without further purification. Hybridization buffer (HB) was 100 mM pH 7.0 phosphate buffered saline (PBS), which was prepared by mixing the stock solutions of NaH_2PO_4 and Na_2HPO_4 (0.2 M) and adjusting the pH with NaOH (0.1 M) and H_3PO_4 (0.1 M). The oligonucleotides were purchased from Sangon Biological Engineering Technology & Co. Ltd. (Shanghai, China) and purified using high-performance liquid chromatography. The sequences were as follows:

cluster template: 5′-CCC ACC CAC CCG CCCA-3′
MB probe: 5′-TTTTTTTTCGCCAATA **TCCTCAGCG**TTTTTTT-3′
Assitant probe: 5′-**CGCTGAGGA***AA* TTT ACGTGCTGCTA-3′

All the RNA sequences were purchased from Shanghai Gene-Pharma Co., Ltd. (Shanghai, China): and purified using high-performance liquid chromatography:

target: 5′-UAGCAGCACGUAAAUAUUGGCG-3′;
single-base mismatch: 5′-UAGCAGCACGUAAAUAUUG**C**CG-3′;
three-base mismatch: 5′-UA**A**CAGCACG**A**AAAUAUUG**C**CG-3′.

2.2. Apparatus and characterization

The morphology of AgNCs was examined with a JEM 2100 transmission electron microscope (TEM) and a multimode 3D atomic force microscopy (AFM) (Bruker, USA). The UV−visible (UV–vis) absorption and X-ray-photoelectron spectroscopy (XPS) analyses were recorded with an UV-1800 spectrophotometer (Shimadzu, Japan) and an ESCALAB 250 spectrometer, respectively. AFM measurement was performed under tapping mode. The sample used for AFM observation was prepared by depositing a droplet of AgCNs dispersion (2 μL) on a freshly cleaved mica surface and dried under vacuum. The image was obtained at room temperature (25 °C) with a humidity of 30%. All fluorescence measurements were performed on a Hitachi F-4500 fluorescence spectrofluorometer (Tokyo, Japan) and temperature was controlled by a D77656 Hoffenberg Huber.

2.3. Preparation of AgNCs

AgNCs were synthesized in accordance with the previous literature (Yeh et al., 2010). Briefly, 50 μL of template strand (100 μM) and 0.8 μL of $AgNO_3$ solution (50 mM) were added to

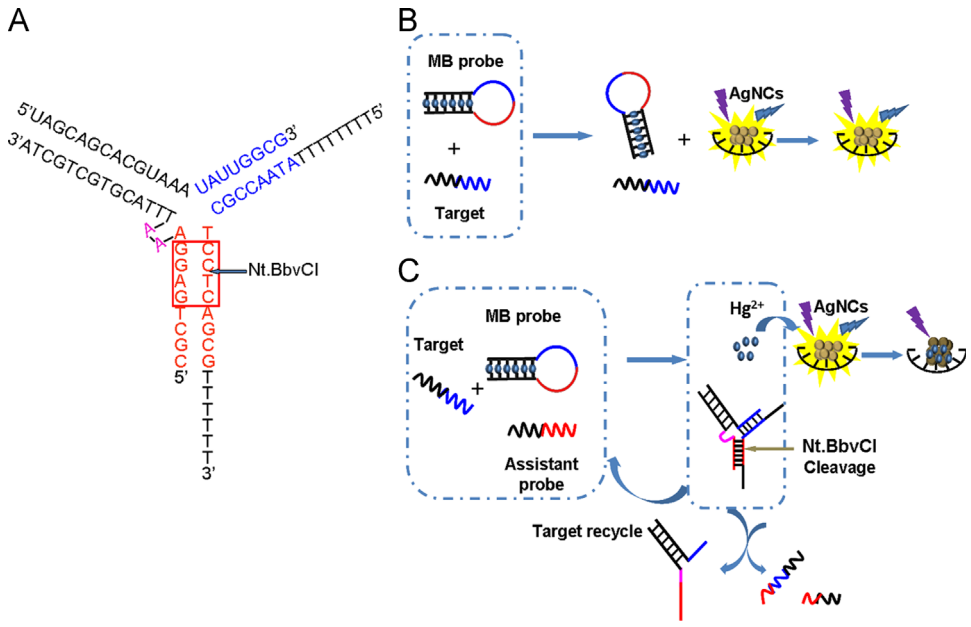

Fig. 1. (A) The Y-shape junction structure of the proposal detection system. Schematic representations of miRNA biosensing based on novel molecular beacon binding readout and target recycling signal amplification in the absence (B) and in the presence of assistant probe (C).

50 μL of citrate buffer (20 mM, pH 7.0), with a $Ag^{+/}$ cluster template relative concentration ratio of 8:1. The mixture was shaken for 10 s, 0.8 μL of fresh $NaBH_4$ solution (25 mM) was then added to the solution maintaining an ice temperature, and the resulting solution was vigorously shaken for 1 min. The oligonucleotide encapsulated AgNCs were obtained by keeping the solution overnight in the dark at 4 °C.

2.4. Interactions of AgNCs with Hg^{2+} ions

To evaluate the fluorescence quenching of AgNCs by Hg^{2+}, 1 μL of Hg^{2+} ions solution with a different concentration was added to 99 μL of AgNCs aqueous solution (1 μM). Fluorescence emission spectra were recorded 2 min later after fully mixing metal ion with the AgNCs. The quenching dynamics was measured as follows: 1 μL of Hg^{2+} solution (42 μM) was added to 99 μL of AgNCs aqueous solution (1 μM). The fluorescence was detected after mixing the solution for 2 min, 5 min, 10 min, 15 min, 20 min, 25 min, 30 min, 40 min, 50 min, and 60 min, respectively.

2.5. Fluorescent miRNA assays

In a typical miRNA assay, 15 μL MB probe (1 μM), 4 μL Hg^{2+} (21 μM), and 1 μL of a different concentration of target miRNA were mixed and diluted to 176 μL of PBS (pH 7.0 100 mM). After the mixture was incubated for ~30 min at 30 °C, 4 μL AgNCs (50 μM) was added to the mixture, the fluorescence emission spectra of AgNCs were then recorded 2-min later. As for specificity measurement, single-base mismatch sequence (10 pM) and three-bases mismatch sequence (10 pM) were performed in the same condition as the target above.

2.6. Endonuclease-assisted target recycle miRNA assays

In order to achieve target-triggered enzymatic recycling amplification, 7.5 μL MB probe (1 μM), 2 μL Hg^{2+} (21 μM), 7.5 μL assistant probe (1 μM), 6 μL NB buffer, 1.5 μL Nt.BbvCI, and 1.5 μL of a different concentration of target miRNA were mixed and diluted to 24 μL of PBS (pH 7.0, 200 mM). After the mixture was incubated for ~1 h at 30 °C, another 50 μL PBS (pH 7.0 100 mM) with AgNCs (2 μM) was added, the fluorescence emission spectra of AgNCs were then recorded 2-min later.

3. Results and discussion

3.1. Characterization of AgNCs

The properties of AgNCs strongly depend on the particles size, stabilizer, surrounding medium, and aggregation state(Yeh et al., 2010; Elisabeth et al., 2008; Garrison and Youngs, 2005; Wipf et al., 1994). In order to obtain the desired AgNCs, the growth of the nanocluster is often encapsulated by a capping agent. The single sequence DNA provides a pre-formed template to stop the nanoclusters from growing once a desired size is reached for the run (Petty et al., 2011; Petty et al., 2012). The morphology of AgNCs obtained were characterized. As shown in Fig. 2A, the AFM image of AgNCs in tapping mode was used to simultaneously collect height and size data. It was observed that the undulate height of AgNCs was about 0.950 nm from the cross-sectional view of the typical AFM image. As shown in Fig. 1A, inset, there were no obvious spots observed from the control AFM image of the same buffer except AgNCs, which indicated the spots of Fig. 1A were AgNCs, not salt. A similar result for the undulate height of AgNCs was also observed in a previous report (Yeh et al., 2010). The cross-sectional view of the typical TEM image exhibited that the prepared AgNCs were almost spherical and the average diameter was approximately 1 nm (Fig. 2B), in agreement with the AFM analysis. XPS was used to confirm the formation of silver from silver nitrate. Fig. 2C illustrates that the XPS in Ag 3d region displayed two strong peaks centered at binding energy of 368 and 374 eV, respectively, indicating the formation of metallic silver (Zhao et al., 2009; Thumu et al., 2010). A strong absorption band was observed at 680 nm from the UV–vis spectrum of the prepared nanostructures (Fig. 2D). It is diverse from the characteristic absorption of the Ag nanoparticle 400 nm (Rodríguez-Sánchez et al., 2005; Dipak et al., 2009), providing further information about the formation of the AgNCs.

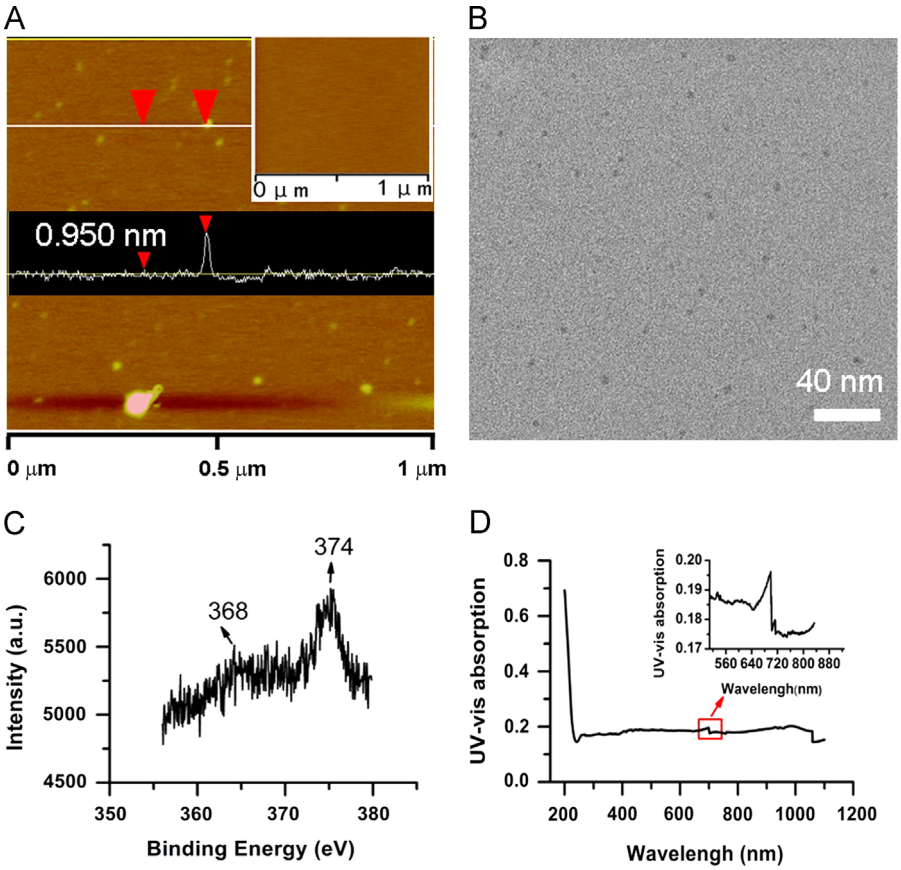

Fig. 2. Characterization of AgNCs: (A) tapping mode AFM image, (B) TEM image, (C) XPS, and (D) UV–vis spectrum of as-prepared AgNCs. Inset A: the AFM image of the same buffer of (A) without AgNCs.

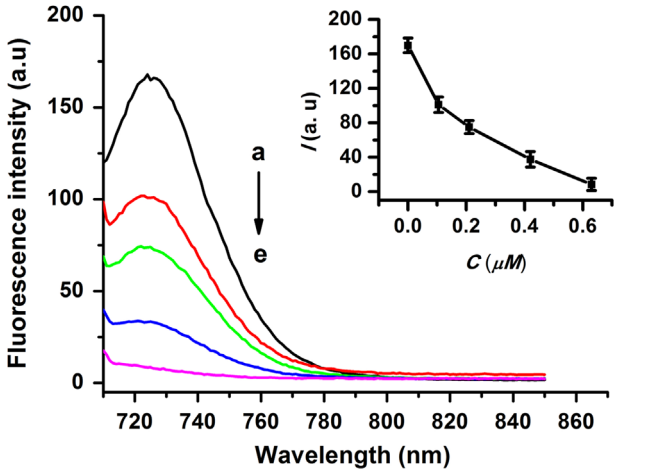

Fig. 3. Fluorescence quenching of AgNCs (1 μM) in the presence of Hg^{2+} with a series of concentrations (a–e: 0, 0.105, 0.21, 0.42, and 0.63 μM). The excitation and the emission wavelengths are 695 and 726 nm, respectively.

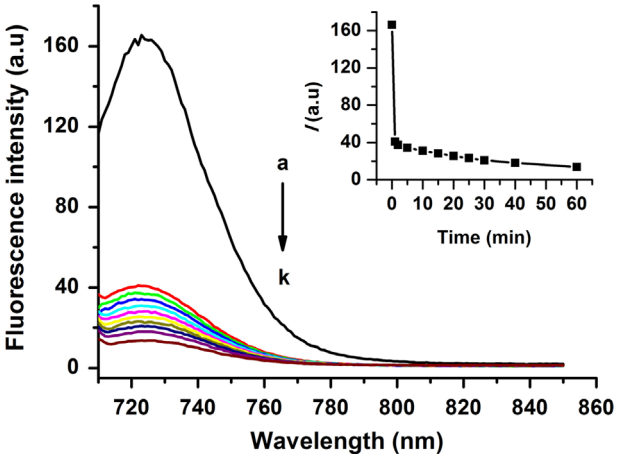

Fig. 4. Fluorescence emission of AgNCs (1 μM) in presence of Hg^{2+} (0.42 μM) as a function of time (a–k: control, 2, 5, 10, 15, 20, 25, 30, 40, 50, and 60 min). The excitation and the emission wavelengths are 695 and 726 nm, respectively.

3.2. *Fluorescence quenching reaction*

It was shown that the fluorescence emission of AgNCs was readily quenched by the Hg^{2+}, which depended on the ratio of fluorescent AgNCs to Hg^{2+} (Guo et al., 2009). As shown in Fig. 3, the fluorescence intensity of AgNCs decreases along with the increase in the concentration of Hg^{2+}. As shown in Fig. 3, inset, the plot of the fluorescence intensity vs. the Hg^{2+} concentration showed that upon addition of 1 μL Hg^{2+} (63 μM) into AgNCs 99 μL (1 μM), the fluorescence of AgNCs was almost completely quenched to 5% of the original fluorescence intensity, which indicated exceptional fluorescent quenching of Hg^{2+}. Fluorescence measurement was further performed to evaluate the quenching kinetics of the Hg^{2+} to the AgNCs. A time-dependent decrease in fluorescence intensity of AgNCs was observed (Fig. 4). From the plot of fluorescence intensity vs time (Fig. 4, inset), it was observed that fluorescence intensity of AgNCs decreased rapidly to 24.8% of original fluorescence intensity in the first 2 min, and then slowly reduced to 8% of the original intensity 1 h-later when 1 μL Hg^{2+} (42 μM) was added into 99 μL AgNCs (1 μM) solution, indicating the strong interaction and fast quenching

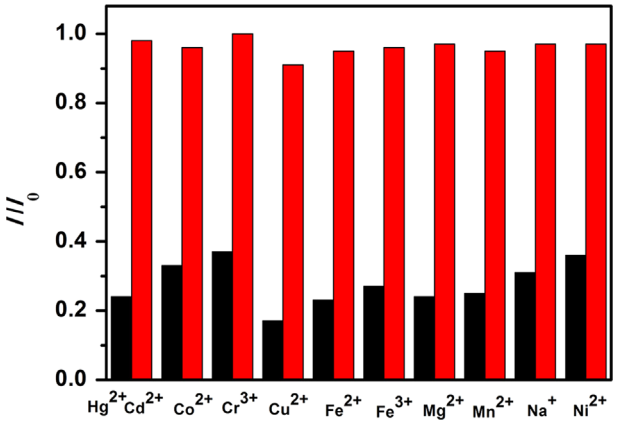

Fig. 5. Fluorescence quenching of AgNCs (1.7 μM) by different metal ions. High columns represent the fluorescence signals of the AgNCs (1.7 μM) in the presence of 0.42 μM of other metal ions. Low columns represent the fluorescence signals of the AgNCs in the presence of 0.42 μM of Hg^{2+} and 0.42 μM of other metal ions. All experiments were performed in duplicate. The excitation and the emission wavelengths are 695 and 726 nm, respectively.

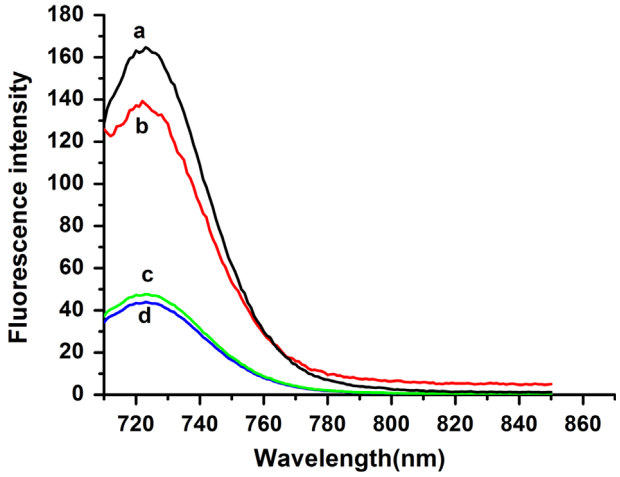

Fig. 6. Fluorescence emission spectra of AgNCs (1 μM) at different experimental conditions: (a) AgNCs in PBS; (b) mixture of Hg^{2+} (0.42 μM) and MB probe (75 nM) PBS containing Hg^{2+} (0.42 μM); (c) mixture containing Hg^{2+} (0.42 μM), MB probe (75 nM) and target (3 nM); (d) PBS containing Hg^{2+} (0.42 μM). The excitation and the emission wavelengths are 695 and 726 nm, respectively.

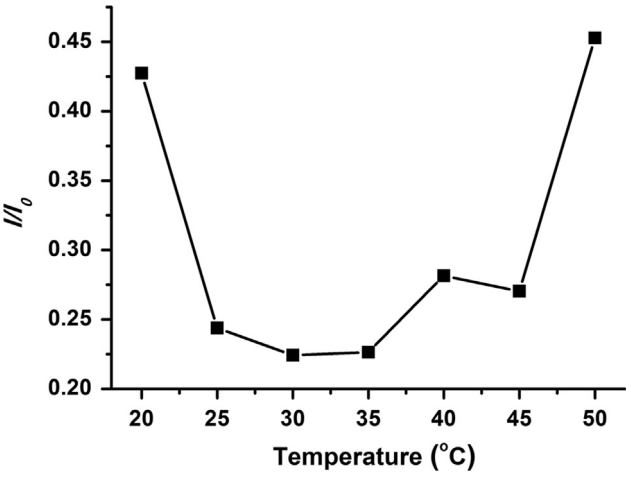

Fig. 7. Fluorescence quenching of AgNCs (1 μM) by released Hg^{2+} in the mixture incubated 1 h for recycling in the presence of 10 pM target (I) and in the absence of target (I_o) at different temperature (20 – 50 °C). The excitation and the emission wavelengths are 695 and 726 nm, respectively.

effect of Hg^{2+} on the fluorescence of AgNCs. The mechanism of the quenching should be that Hg^{2+} would also quench the fluorescence of AgCNs via the d^{10}–d^{10} metallophilic interaction ($5d^{10}(Hg^{2+})$ –$4d^{10}(Ag^{+})$) (Guo and Joseph, 2011).

To test the specificity of the quenching effect of Hg^{2+} on the fluorescence of AgNCs, other metal ions were used in the place of Hg^{2+}. The relative fluorescence intensity signal in the absence or presence of Hg^{2+} was measured. In the absence of Hg^{2+}, none of the tested metal ions could result in an obvious signal decrease (Fig. 5). Meanwhile, Cu^{2+}, Fe^{2+}, Fe^{3+}, Mn^{2+}, Mg^{2+} and Cd^{2+} ions presented slight quenching effects on the fluorescence of the AgNCs. When 0.42 μM of Hg^{2+} and 0.42 μM of another metal ion were both added to the test solution, the signal of the sensor increased to a level similar to when Hg^{2+} alone was added. Meanwhile, the AA and UA also show negligible interference. These results demonstrated the high selectivity of this sensing system for detecting Hg^{2+}, which indicated great potential for future use.

To investigate the possibility of developing a novel miRNA sensing system based on the quenching, fluorescence emission spectra of AgNCs in different conditions were first studied. It demonstrated that the hybridization of the target with the MB probe disturbed the T–Hg^{2+}–T structure and the Hg^{2+} was effectively released into the solution (Fig. 6), and the released Hg^{2+} could then quench the fluorescence of the AgNCs.

3.3. Target recycling amplification

The temperature employed for target recycling is selected to meet the requirement that efficiently triggers recycling in the presence of the target, while avoiding triggering recycling in the absence of target to reduce the false positive signal. As shown in Fig. 7, the signal-to-noise ratio is best at 30 °C. It demonstrated that the target could not effectively displace the Hg^{2+} and trigger recycling amplification when the temperature was lower than 30 °C, and the T–Hg^{2+}–T structure would become unstable when the temperature increased to 40 °C. Thus, the 30 °C was selected for target recycling amplification.

3.4. miRNA assay performance

The comparison of the performances of the assay with or without target recycling amplification is shown in Fig. 8. In the absence of target recycle, the fluorescence emission signal gradually decreased along with the concentration increase of target miRNA used for hybridization. The plot of the fluorescence intensity obtained by four times measurements of each sample showed a good linear relationship with the target concentration covering the range of from 0.5 to 50 nM (Fig. 8A inset, error bar: SD, N=4). The limit of detection (LOD) for target miRNA was estimated to be 0.16 nM at 4 times the standard deviation obtained by four times repeated measurements of buffer without target miRNA. The sensitivity is greater than or close to the MB-based nucleic acid detection with a LOD at nanomolar level (Lee et al., 2008; Nguyen and Anslyn, 2006), probably resulting from the high signal-to-noise ratio. After introducing the signal amplification strategy, the assay showed an ultrasensitive homogeneous detection of miRNA down to sub-femtomolar level (0.6 fM) with a good linear range of 5 orders of magnitude (from 10 pM ~ 1 fM). Upon the continuous decrease of the concentration of target to 0.1 fM, the fluorescence intensity leveled off. (Fig. 8B inset, error bar: SD, N=4). It demonstrated that the endonuclease-assistant target recycling amplification effectively improved both the sensitivity and dynamic linear range.

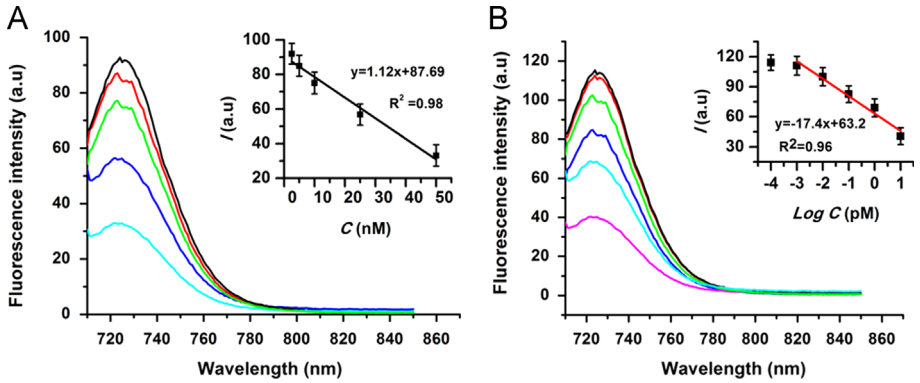

Fig. 8. (A) Fluorescence emission spectra of AgNCs (1 μM) after incubation mixture containing target at different concentrations (50, 25, 10, 5, 0.5 nM). (B) Fluorescence emission spectra of AgNCs (1 μM) in the mixture with different target concentration (10 pM–1 fM) incubated for target recycling 1 h, other conditions as described in (A). Inset: plot of fluorescent intensity *I* vs. target concentration, error bar: SD, $N=4$. The excitation and the emission wavelengths are 695 and 726 nm, respectively. (For interpretation of the references to color in this figure, the reader is referred to the web version of this article.)

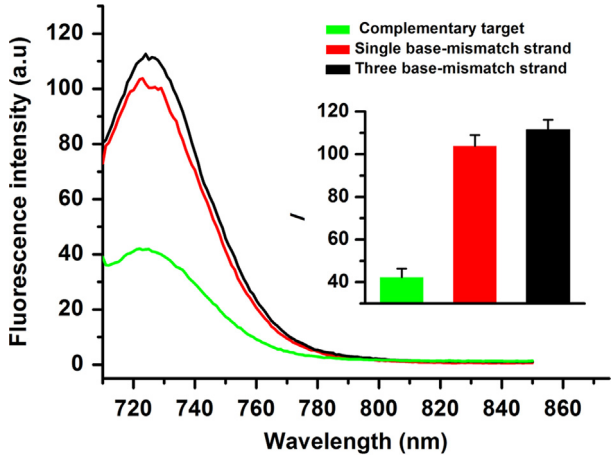

Fig. 9. Fluorescence emission spectra of AgNCs (1 μM) in mixture containing different 10 pM strands (complementary target, single-base mismatch strand, three-base mismatch strand), MB probe (75 nM) and Hg^{2+} (0.42 μM) 2-min later. Fluorescence intensity *I* for these cases. The excitation and the emission wavelengths are 695 and 726 nm, respectively.

In comparison with the linear DNA probe, MB exhibits significant advantage in the specific target detection. The coordination chemistry of thymine–Hg^{2+}–thymine complexes (T–Hg^{2+}–T) also provides an emerging approach for biomolecular detection due to the strong and stable duplex structure (Zhang et al., 2013; Ye and Yin, 2008; Huy et al., 2011). To investigate the mercury ion-meditated MB and whether it kept the inherent specificity for target detection, three kinds of miRNA sequences including perfectly complementary target, single-base mismatched strand, and three-base mismatched strand were studied in the same condition. The proposed system exhibited a high capability of discriminating between a perfectly complementary target and the mismatched stands (Fig. 9). As shown in Fig. 8, inset, the perfectly complementary target (inset, histograms green) showed an *I* value of 41% that for single-base mismatch sequence (inset, histograms red), while the response to the three-base mismatch stand (inset, histogram black) was 2.63-folds of that for the perfectly complementary target. It suggested that the strategy has high fidelity in discriminating single-base mismatch due to the competition displacing the interaction between the target and the Hg^{2+}. Furthermore, the interferences from the some commonly seen metal ions and small molecules show negligible influence (date not shown), which reasoned from the specificity of quenching effect of Hg^{2+} on the fluorescence of AgNCs. Essentially, the selectivity of the ion-meditated conformational MB could be further improved by adjusting the concentration of metal ions (Li et al., 2000; Tang et al., 2005).

4. Conclusions

In conclusion, we have developed a novel strategy for the facile and ultrasensitive detection of miRNA by integrating a label-free mercury ion-meditated conformational MB using fluorescent AgNCs as reporter and endonuclease-assistant target recycling amplification. The resulting AgNCs with narrow size-distribution were characterized by AFM, TEM, UV–vis, and XPS. The interaction between the AgNCs and Hg^{2+} was investigated, and the high fluorescence quenching efficiency of Hg^{2+} to AgNCs and endonuclease-assistant target recycling amplification allow the biosensor to detect the target with higher sensitivity in comparison to analogous homogenous solution nucleic acid detection. The competition displacing interaction between the target and the Hg^{2+} facilitated the assay to discriminate sequence mutant, while the ion-meditated conformational MB-based signal readout strategy avoided any laborious labeling. These features establish the simplicity, validity, and universality of the detection platform, opening a new avenue for bioanalysis.

Acknowledgment

This work was funded by China Postdoctoral Science Foundation (No. 11175012, 11175039), Postdoctoral Special Foundation (No. 2012T50042), the National Natural Science (NO. 21305008), the Chinese Central Universities Funds (No. 06199017), the National Natural Science Foundation of China (No. 21127007), Ph.D. Programs Foundation of Ministry of Education of China (No. 20120006120006).

References

Ambros, V., 2004. Nature 431, 350–355.
Bartel, D.P., 2004. Cell 116, 281–297.
Bonanni, A., Pumera, M., 2011. ACS Nano 5, 2356–2361.
Calin, G.A., Croce, C.M., 2006. Nature Reviews Cancer 6, 857–866.
Cissell, K.A., Shrestha, S., Deo, S.K., 2007. Analytical Chemistry 79, 4754–4761.
Dipak, K.B., Harekrishna, B., Priyanka, S., Gobinda, P.S., Sankar, P.D.M., Ajay, J., 2009. Journal of Molecular Liquids 145, 33–37.
Dong, H.F., Gao, W.C., Yan, F., Ji, H.X., Ju, H.X., 2010. Analytical Chemistry 82, 5511–5517.
Dong, H.F., Zhang, J., Ju, H.X., Lu, H.T., Wang, S.Y., Jin, S., Hao, K.H., Du, H.W., Zhang, X.J., 2012a. Analytical Chemistry 84, 4587–4593.
Dong, H.F., Jin, S., Ju, H.X., Hao, K.H., Xu, L.P., Lu, H.T., Zhang, X.J., 2012b. Analytical Chemistry 84, 8670–8676.

Duan, H.W., Nie, S.M., 2007. Journal of the American Chemical Society 129, 2412–2413.
Dyadyusha, L., Yin, H., Jaiswal, S., Brown, T., Baumberg, J.J., Booy, F.P., Melvin, T., 2005. Chemical Communications 25, 3201–3203.
Elisabeth, G.G., Patrick, O.J., Anthony, G., Dave, B., Deborah, K.F., 2008. Advanced Materials 20, 279–283.
Garrison, J.C., Youngs, W.J., 2005. Chemical Reviews 105, 3978–4008.
Guo, C.L., Joseph, I., 2011. Analytical Chemistry 83, 2883–2889.
Guo, W.W., Yuan, J.P., Wang, E.K., 2009. Chemical Communications, 3395–3397.
He, L.G., Hannon, J., 2004. Nature Reviews Genetics 5, 522–531.
Huy, D.G., Zhang, M., Zuo, P., Ye, B.C., 2011. Analyst 136, 3289–3294.
Jay, C., Nemunaitis, J., Chen, P., Fulgham, P., Tong, A.W., 2007. Cell Biology 26, 293–300.
Jeffrey, S.S., 2008. Nature Biotechnology 26, 400–401.
Kumar, M.S., Lu, J., Mercer, K.L., Golub, T.R., Jacks, T., 2007. Nature Genetics 39, 673–677.
Lee, K., Maisel, K., Rouillard, J., Gulari, E., Kim, J., 2008. Chemistry of Materials 20, 2848–2850.
Lewis, B.P., Burge, C.B., Bartel, D.P., 2005. Cell 120 (1), 15–20.
Li, J.J., Geyer, R., Tan, W.H., 2000. Nucleic Acids Research 28, e52.
Liu, Y.Q., Zhang, M., Yin, B.C., Ye, B.C., 2012. Analytical Chemistry 84, 5165–5169.
Lu, J., Getz, G., Miska, E.A., Alvarez–Saavedra, E., Lamb, J., Peck, D., Sweet–Cordero, Mallory, A.C., Vaucheret, H., 2006. Nature Genetics 38 (Suppl 1), S31–S36.
Mallory, A.C., Vaucheret, H., Nat. Genet. 2006, 38 (Suppl 1), S31–S36.
Marras, S.A.E., 2006. Methods in Molecular Biology 335, 3–16.
Nelson, P.T., Baldwin, D.A., Scearce, L.M., Oberholtzer, J.C., Tobias, J.W., Mourelatos, Z., 2004. Nature Methods 1, 155–161.
Nguyen, B.T., Anslyn, E.V., 2006. Coordination Chemistry Reviews 250, 3118–3127.
Oh, E., Hong, M.Y., Lee, D., Nam, S.H., Yoon, H.C., Kim, H.S., 2005. Journal of the American Chemical Society127, 3270–3271.
Pall, G.S., Codony–Servat, C., Byrne, C.J., Ritchie, L., Hamilton, A., 2007. Nucleic Acids Research 35 (8), e60.
Pasquinelli, A.E., Hunter, S., Bracht, J., 2005. Current Opinion in Genetics & Development 15, 200–205.
Petty, Jeffrey, T., Story, S.P., Juarez, S., Votto, S.S., Herbst, A.G., Degtyareva, N.N., Sengupta, B., 2012. Analytical Chemistry 84, 356–364.
Petty, Jeffrey T., Sengupta, B., Story, S.P., Degtyareva, N.N., 2011. Analytical Chemistry 83, 5957–5964.
Plasterk, R.H., 2006. Cell 124, 877–881.
Rao, T.U.B., Pradeep, T., 2010. Angewandte Chemie International Edition 49, 3925–3929.
Rodríguez-Sánchez, M.L., José, R.M., Blanco, M.C., José, R., López Quintela, M.A., 2005. Journal of Physical Chemistry 109, 1183–1191.
Sokol, D.L., Zhang, X., Lu, P., Gewirtz, A.M., 1998. Proceedings of the National Academy of Sciences of the United States of America 95, 11538–11543.
Tang, Z.W., Wang, K.M., Tan, W.H., Ma, C.B., Li, J., Liu, L.F., Guo, Q.P., Meng, X.X., 2005. Nucleic Acids Research 33, e97.
Thumu, B.R., Bodappa, N., Thalappil, P., 2010. Journal of the American Chemical Society 132, 16304.
Tricoli, J.V., Jacobson, J.W., 2007. Cancer Research 67, 4553–4555.
Tyaji, S., Kramer, F.R., 1996. Nature Biotechnology 14, 303–308.
Wark, A.W., Lee, H.J., Corn, R.M., 2008. Angewandte Chemie International Edition 47, 644–652.
Wang, K.M., Tang, Z.W., Yang, C.Y.J., Kim, Y.M., Fang, X.H., Li, W., Wu, Y.R., Medley, C. D., Cao, Z.H., Li, J., Colon, P., Lin, H., Tan, W.H., 2009. Angewandte Chemie International Edition 48, 856–870.
Wang, Y.X., Li, J.S., Wang, H., Jin, J.Y., Liu, J.H., Wang, K., Tan, M., Yang, W.H., R.H, 2010. Analytical Chemistry 82, 6607–6612.
Wipf, P., Venkatraman, S., Miller, C.P., Geib, S.J., 1994. Angewandte Chemie International Edition 106, 1554–1556.
Ye, B.C., Yin, B.C., 2008. Angewandte Chemie International Edition 47, 8386–8389.
Yeh, H.C., Sharma, J., Han, J.J., Martinez, J.S., Werner, J.H., 2010. Nano Letters 10, 3106–3311.
Zhang, M., Le, H.N., Jiang, X.Q., Ye, B.C., 2013. Chemical Communications 49, 2133–2135.
Zhao, B., Liu, Z.R., Liu, Z.L., Liu, G.X., Li, Z., Wang, J.X., Dong, X.T., 2009. Electrochemistry Communications 11, 1707–1710.
Zheng, J., Nicovich, P.R., Dickson, R.M., 2007. Annual Review of Physical Chemistry 58 (409), 409–431.